HHS Public Access

Author manuscript

Magn Reson Med. Author manuscript; available in PMC 2019 February 01.

Published in final edited form as:

Magn Reson Med. 2018 February ; 79(2): 806–814. doi:10.1002/mrm.26736.

Amide Proton Transfer CEST of the Cervical Spinal Cord in Multiple Sclerosis Patients at 3T

Samantha By[1,2], **Robert L. Barry**[3,4], **Alex K. Smith**[1,2,5], **Bailey D. Lyttle**[2], **Bailey A. Box**[2], **Francesca R. Bagnato**[6], **Siddharama Pawate**[6], and **Seth A. Smith**[1,2,7]

[1]Department of Biomedical Engineering, Vanderbilt University, Nashville, TN, USA

[2]Vanderbilt University Institute of Imaging Science, Vanderbilt University Medical Center, Nashville, TN, USA

[3]Athinoula A. Martinos Center for Biomedical Imaging, Department of Radiology, Massachusetts General Hospital, Charlestown, Massachusetts, USA

[4]Department of Radiology, Harvard Medical School, Boston, Massachusetts, USA

[5]Functional MRI of the Brain Centre, Nuffield Department of Clinical Neurosciences, University of Oxford, Oxford, UK

[6]Department of Neurology, Vanderbilt University Medical Center, Nashville, TN, USA

[7]Department of Radiology and Radiological Sciences, Vanderbilt University Medical Center, Nashville, TN, USA

Abstract

Purpose—The ability to evaluate pathological changes in the spinal cord in multiple sclerosis (MS) is limited, as T_1- and T_2-w MRI imaging is not sensitive to biochemical changes in vivo. Amide proton transfer (APT) chemical exchange saturation transfer (CEST) can indirectly detect amide protons associated with proteins and peptides, potentially providing more pathological specificity. Here, we implement APT CEST in the cervical spinal cord of healthy and MS cohorts at 3T.

Methods—APT CEST of the cervical spinal cord was obtained in a cohort of 10 controls and 10 MS patients using a novel respiratory correction methodology. APT was quantified using two methods: 1) APT_w, based off of the conventional magnetization transfer ratio (MTR) asymmetry and 2) ΔAPT, a spatial characterization of APT changes in MS patients relative to the controls.

Results—Respiratory correction yielded highly reproducible z-spectra in white matter (ICC=0.82). APT_w signals in normal appearing white matter (NAWM) of MS patients were significantly different from healthy controls (P=0.04), while ΔAPT maps of MS patients highlighted large APT differences in NAWM.

Contact Info for Corresponding Author. Seth Smith, Associate Professor, 1161 21st Avenue South, Nashville, TN, phone: 615-322-6211, seth.smith@vanderbilt.edu.

Conclusion—Respiration correction in the spinal cord is necessary to accurately quantify APT CEST, which can provide unique biochemical information regarding disease processes within the spinal cord.

Keywords

amide proton transfer; CEST; multiple sclerosis; spinal cord; normal appearing white matter

Introduction

The spinal cord is exceptionally involved in multiple sclerosis (MS) (1), however, the ability to assess and characterize spinal cord disease using conventional magnetic resonance imaging (MRI) is limited. Clinical MRI sequences are often not sensitive and lack specificity for the underlying pathological changes known to occur in MS. Conventional T_1- and T_2- weighted imaging can detect lesions when the water content has changed, and has been shown to be sensitive to inflammation or necrosis and atrophy (2,3), yet lacks the ability to detect sub-voxel biochemical or cellular changes in vivo (4). Additionally, because necrosis and atrophy are late-stage manifestations of MS, an improved set of imaging biomarkers capable of providing greater pathological specificity earlier in the disease process (ideally even before inflammation becomes apparent) may have significant clinical implications for disease monitoring, treatment, and prognosis.

Chemical exchange saturation transfer (CEST) is an MRI method that indirectly detects mobile species with exchangeable protons (5). In a CEST experiment, low power radiofrequency (RF) irradiation is used to selectively saturate (at a spectrally selective offset frequency with respect to water) the labile protons associated with these mobile moieties. Thus, through direct chemical exchange, the bulk water signal is attenuated (6). In vivo, the magnitude of this exchange-mediated attenuation is a function of exchange rate, concentration of the labile protons, pH, and saturation efficiency, but can also be influenced by confounding relaxation effects and other exchange phenomena (i.e. magnetization transfer, MT and nuclear overhauser, NOE). When performing RF irradiation at multiple offset frequencies, a so-called CEST z-spectrum (7) is generated: a normalized signal as a function of the saturation offset frequency (Δω) with respect to water. Conventionally, the CEST z-spectrum is a narrow, asymmetric lineshape, if the assumption of slow exchange on the MR timescale (i.e. solute to water exchange rate k_{sw} < chemical shift of the labile protons) is met (8). The most often reported CEST effect in vivo is amide proton transfer (APT) CEST, which is sensitive to the backbone amide protons associated with proteins and peptides resonating at 3.5 ppm downfield from water (5,9–11).

Though APT CEST promises valuable information for studying the human spinal cord, several challenges hamper its application in vivo. In addition to the small size of the cord itself, the close proximity of the lungs (respiration) and heart (cardiac cycle), along with the pulsating cerebrospinal fluid, creates motion artifacts that are difficult to correct. Furthermore, respiration-induced field shifts can dynamically distort the B_0 field in the spinal cord and cause temporal signal fluctuations, with field shifts up to 0.58 ppm shift at C7 as reported by Verma et al. (12). These field shifts are especially problematic for CEST,

since spectrally accurate RF irradiation is required to generate CEST contrasts and quantification of CEST relies on deviation of the signal from a consistent baseline signal. However, currently, no standard approaches to correct for respiration effects in CEST applications to the cervical spinal cord exist.

This work aims to evaluate the potential for a novel post-processing respiratory correction scheme to mitigate respiratory artifacts on quantitative CEST measurements in the human cervical spinal cord. We apply the proposed method in both healthy volunteers and patients with MS at 3T, showing for the first time that APT CEST in the cervical spinal cord can offer unique biochemical information.

Methods

MRI Experiments

Ten age-matched healthy volunteers participated in this study (5M/5F, 24–58 years, mean 35.6 years), five of whom were scanned twice within three weeks to assess reproducibility. Ten patients with MS (4M/6F, 30–60 years, mean 43.9 years, 9 RRMS, 1 PPMS) were enrolled in this study and patients' disability was rated using the Expanded Disability Status Scale (EDSS) score (13). All patients met the revised McDonald criteria (14) at the time of the study; additionally, all patients had brain lesions suggestive of MS. Clinical and demographic details of patients are listed in Table 1. Local institutional review board and written informed consent was obtained prior to imaging. Imaging was acquired using a 3.0T whole body MR scanner (Philips Achieva). A quadrature body coil was used for excitation and a 16-channel SENSE neurovascular coil was used for reception.

For each subject, a high-resolution ($0.65\times0.65\times5\ mm^3$) multi-slice, multi-echo gradient echo (mFFE) anatomical image (15) was acquired (TR/TE/ΔTE = 753/7.1/8.8 ms, $\alpha = 28°$, number of slices=14, 6:12 min) for co-registration and to serve as a template for segmentation.

The CEST sequence consisted of a gradient-echo, with a multi-shot echo planar imaging (EPI) readout (EPI factor = 7). A single slice (slice thickness = 20 mm) was obtained, centered at the C3/C4 level. CEST saturation was achieved with a shaped 2 μT pulse (a single 150 ms RF Gaussian pre-pulse), applied at 36 asymmetric offsets (Δω) sampled between +/− 5 ppm (with greater density of samples around the APT resonance). After every third off-resonance saturation, an interleaved non-saturated scan (S_0, Δω = 100,000 Hz) was acquired for reference, yielding a total of 13 S_0 images. Additional relevant parameters for the CEST sequence include: FOV = 160mm × 160mm, voxel size = 1mm × 1mm, SENSE = 2 (RL), TR/TE = 305/12 ms, $\alpha = 20°$, ProSet fat suppression, NSA = 5. The sequence was designed such that steady-state was reached at the center of k-space (16). Total acquisition time was 13:45 minutes.

For each CEST acquisition, a water saturation shift referencing (WASSR) (17) scan was also acquired for static B_0 correction. For WASSR, a 0.5 μT, 200 ms saturation pulse applied at $\Delta\omega = +/-1$ppm in increments of 0.1 ppm with the following parameters: TR/TE = 405/7.9 ms, voxel size = 1.5mm × 1.5mm, NSA = 1, acquisition time=1:25 min. For all subjects, the

respiratory cycle was externally monitored and recorded using a respiratory bellows placed on the abdomen.

To demonstrate that the proposed respiration correction method (See *Methods: Image Processing & Analysis*) does not produce any adverse effects, a phantom comprised of egg whites was prepared and imaging was performed identical to the sequences used on the human subjects (18). The respiratory cycle was monitored on a healthy volunteer that was seated outside of the scanner using the respiratory bellows.

Image Processing & Analysis

The image processing pipeline is summarized in Figure 1 and can be broken down into 4 steps: 1) Registration, 2) Segmentation, 3) Respiration Correction, and 4) CEST Analysis.

1. To account for any motion occurring during the sequence, each CEST and WASSR volume was diffeomorphically registered to the mFFE using Advanced Normalization Toolbox (ANTs) (19).
2. White matter (WM) and gray matter (GM) were automatically segmented from the co-registered mFFE image using a slice-based, groupwise multi-atlas procedure (20). In patients, lesions were inspected slice-wise on the mFFE and then manually delineated on the averaged mFFE slices covering the CEST volume. By delineating lesions on the averaged mFFE, some voxels containing lesional tissue were likely averaged out; however, this process ensured not averaging in any normal voxel in the region of interest. Lesion determination and delineation were confirmed by an MS clinician (FB).
3. For each CEST acquisition, the 13 S_0 images were spline interpolated as a function of time, and consequently, the signal intensities for each CEST-weighted image ($S(\Delta\omega)$) at each offset were normalized by that spline-interpolated S_0 (21). To correct for signal fluctuations due to respiration, the respiration volume per unit time (RVT) was calculated from the bellow recording (22). Due to a dynamic scan time of 16 seconds, multiple respiratory cycles occurred during the acquisition of each CEST image, and therefore required a regressor that reflected changes in the depth and rate of breathing. For the acquisition of each CEST image, the RVT was calculated by dividing the range of the bellows magnitude recording (maximum-minimum throughout the entire dynamic) with the respiration period (mean time between respiratory peaks). To account for the global effect of respiration on the overall CEST z-spectrum acquisition, the RVT was then scaled by the range of the signal drift in all of the S_0 images and regressed out of the CEST data. For comparison, the CEST data was also processed using two methods: a) “No Correction”, which does not account for respiration effects, using only the average of the first and last S_0 image for normalization and b) “Jones Method”, which only compensates for signal fluctuations by using the spline-interpolated S_0 (21).
4. To correct for static B_0 field inhomogeneities, the mean absolute water frequency shift was calculated from the WASSR scan voxel-by-voxel and the CEST z-

spectrum was shifted accordingly. The APT CEST effect was calculated using a form of the conventional APT asymmetry (23), but rather than taking a single point, the area under the curve from both the positive and negative side were used:

$$\mathrm{APT}_w = \frac{\int_{-3\ \mathrm{ppm}}^{-4\ \mathrm{ppm}} 1 - S(\Delta\omega)d\omega - \int_{3.2\ \mathrm{ppm}}^{3.8\ \mathrm{ppm}} 1 - S(\Delta\omega)d\omega}{S_0} \quad (1)$$

The APT_w signal is expressed in units of percent. Note a wider range of integration was used on the negative side due to the asymmetric sampling scheme implemented in order to finely sample the APT signal. This resulted in sparser sampling (with larger integration width) on the negative side, however previous studies have demonstrated that the NOE signal is slowly varying (21), and therefore the chosen sampling scheme should not significantly affect the observed APT_w values.

Repeatability

Reproducibility of the z-spectrum was assessed using the intraclass correlation coefficient (ICC) for both CEST quantification methods and in both WM and GM separately. To estimate the ICC, each control contributed six points from the z-spectrum ($\Delta\omega$ = 3.2–3.8 ppm), where each point was a mean value over all of the voxels in a given ROI The 95% confidence intervals (CI) for the ICC were calculated using a bootstrap procedure.

Group Comparison

A non-parametric Wilcoxon rank sum test was performed to evaluate group differences in the mean APT_w values between healthy WM and all WM (both NAWM and lesions) for MS patients at a significance threshold of α=0.05. Histograms of APT_w values in WM were created for both cohorts, with the MS cohort grouped by EDSS score. Mean, median, skewness and overlap of the histograms were calculated.

Spatial Differences Between Cohorts

To assess spatial differences between the MS and control cohorts, APT difference (ΔAPT) maps were calculated. For this method, to remove any possible confounding factors from NOE (24) or MT effects, which are known to be different in MS patients compared to healthy controls (25,26), only the positive side of the z-spectrum downfield from water ($\Delta\omega$ = +3.2–3.8 ppm) was assessed. Similar to Eq (1), APT was calculated as the integrated area over a region of the curve, but only the positive side was used (+APT, units in percent). The anatomical images from each subject in the control cohort were diffeomorphically registered to one another and the transformation was then applied to the calculated +APT maps from each subject. With all data in a standard space, the calculated +APT maps were averaged over all control subjects. The mean APT over all of the controls was calculated and subtracted on a voxel-by-voxel basis from the +APT map for each MS patient. Therefore,

the absolute ΔAPT represents an absolute signal change in patients with respect to controls. Mean absolute ΔAPT values were derived from NAWM and lesions for each patient.

Results

Respiration Correction Improves CEST Signal Reproducibility

Relatively large signal fluctuations in the measured, interspersed S_0 images were observed in all controls for WM (mean peak-to-peak range=14.2%, max=25.8%, min=8.4%) and GM (mean=13.5%, max=23.5%, min=5.62%). Consequently, the reproducibility of the z-spectrum was low for the uncorrected data, yielding an ICC (95% CI) of 0.45 (0.20, 0.61) and 0.36 (0.10, 0.57) for WM and GM, respectively. With the Jones method (spline interpolation of S_0 only), the reproducibility of the z-spectrum improved but still remained low, resulting in an ICC of 0.57 (0.40, 0.70) and 0.58 (0.39, 0.74) for WM and GM, respectively. After applying our respiration correction scheme, the z-spectrum showed the highest level of reproducibility with an ICC of 0.82 (0.73, 0.89) and 0.79 (0.67, 0.87) for WM and GM, respectively. Additionally, as observed in Figure 2, the respiration correction shows a noted APT CEST effect around the resonance of interest ($\Delta\omega$ = +3.5 ppm). Without any correction (black), the features of the mean z-spectrum over WM is confounded by physiological noise, producing a more symmetric z-spectrum with a reduced APT effect (WM mean=20.6±2.01%); with the Jones method, the APT effect was similar (WM mean=20.3±1.76%); with the proposed respiration correction (blue), the z-spectrum is more asymmetric and an increased APT effect is observed (WM mean=24.1±2.40%). Furthermore, the corrected z-spectrum provides a more profound MT effect, which is expected in the WM of the spinal cord (25).

Most importantly, without a feasible gold standard for comparison (see Discussion), it is necessary to prove that our post-processing respiration correction does not produce any spurious APT effects. Figure 3 plots the z-spectrum of the egg white phantom — uncorrected, corrected using the Jones method and corrected with our proposed method — with the respiratory recording of a person outside of the scanner, and demonstrates good agreement between all three methods (ICC≥0.99 for all comparisons), indicating that the respiration correction does not inadvertently produce a non-existent CEST effect.

Application to MS Cohort

Figure 4 highlights the ability to capture the heterogeneity in the distribution of the observed APT effects in MS with APT CEST. Note that the rest of the data (both patients and controls), unless otherwise noted, is shown with respiration correction. Figure 4a shows the histogram of APT_w values over all WM for healthy controls and patients (including both lesions and NAWM). There is a slight decrease in mean and median APT_w in the MS cohort (mean=15.5%, median=14.7%) in comparison to the controls (mean=17.5%, median=16.7%), but the histograms of each cohort overlaps one another by 44.5% and follow an approximately normal distribution (skewness: controls=0.29, MS=0.46). Classifying the WM in the MS cohort identifies a distinction between APT_w signals for NAWM and lesions, however the difference is minimized due to the histograms containing

more NAWM voxels in patients with an EDSS score of 0, and therefore we separated the cohorts by EDSS score.

In the cohort of five MS patients with an EDSS of 0 (Figure 4b), the overlap with the control histogram remains large (43.2%) and it is difficult to separate either lesions or NAWM from the controls ($P>0.2$); however, when considering the five patients with an EDSS greater than 0 (Figure 4c), the overlap decreases to 36.2% and a binomial distribution is observed for the MS cohort, which we believe is reflective of different tissue characteristics in lesions and NAWM in patients showing disability. It is worth noting that a significant difference exists between the NAWM ($P=0.04$) and control WM, whereas the same trend is nonexistent in lesions ($P>0.05$), as shown in Table 2.

Given the possible confounding effects of NOE and MT, we considered the ΔAPT to localize the magnitude and spatial distribution of APT changes in the spinal cord of the MS patients relative to healthy controls. Figure 5 includes the anatomical image with the lesion outlined in black (left), ΔAPT maps (middle), and z-spectrum (right) for five MS patients with varying degrees of EDSS scores and disease duration. For reference, the mean z-spectrum over all controls is plotted in black, with standard deviation over all controls shown in shaded gray. The mean absolute ΔAPT in WM in MS patients with respect to controls (mean +APT=23.8±1.73%) was found to be 3.05%. In MS 4 (EDSS=0, 6 years), the mean difference is only 1.16% throughout the NAWM. The heterogeneity of MS pathology, however, is clearly evident with APT CEST in the ΔAPT maps for patients with higher EDSS scores or longer disease durations. Large differences in mean absolute ΔAPT are observed in the NAWM of MS 5 (5.50% vs 0.84% for lesion), a patient with EDSS=2 and duration of disease of 17 years, and MS 6 (4.07% vs 1.41%), a patient with EDSS=4.5 and duration of disease of 22 years. In MS 10 (EDSS 6, 10 years), a large difference in mean absolute ΔAPT was seen throughout the cord of 8.41%. In MS 3 (EDSS=3.5, 4 years), areas of increased APT around the border of the lesion are observed. Furthermore, it is important to note that these observed ΔAPT changes correspond well with focal signal intensity differences in the z-spectrum at 3.5 ppm for lesions (red) and NAWM (blue).

Discussion

Our results demonstrate (1) the ability to provide more reproducible CEST z-spectrum in the spinal cord of healthy controls using a novel offline respiratory correction method and (2) the ability of respiratory-corrected APT CEST to show signal differences between healthy controls and patients with MS.

Respiration Correction

To date, only two studies have utilized APT CEST to study MS. Notably, Dula et al. performed a preliminary study in the brain of MS patients at 7T, reporting disparity between controls and patients in NAWM, along with heterogeneity between different lesions (27). Despite its potential, APT CEST has never been applied to the spinal cord at 3T, let alone in any pathology, and the first attempt at APT CEST in the spinal cord was only recently performed, but at 7T (28). Translation of APT CEST to areas outside of the brain introduces technical challenges that have been currently unaddressed. In particular, we observed that

the effects of respiration on quantifying APT were too significant to ignore and ultimately removed any sensitivity to the APT effect. Conventional prospective respiration compensation methods were not feasible to implement, since respiratory gating would increase the scan time and with respiratory triggering, a time-varying TR may prevent steady state from being reached or maintained during the acquisition window. Therefore, an image-based retrospective correction method was proposed.

Methods to correct for the detrimental effects of physiological noise have been standard practice in functional MRI (fMRI) experiments for over two decades (29–31). Many fMRI image-based correction methods, such as RETROICOR, assume that a unique respiratory phase can be assigned to each acquired image (29), but this assumption was inadequate as each dynamic of our CEST sequence was 16 seconds. Our proposed method is a novel extension of spline interpolation, previously implemented to correct for signal drift (21), but further accounts for respiration by detrending the RVT. Since multiple respiratory cycles are present during each image acquisition, the magnitude of the respiration was an insufficient regressor. In the future, more elaborate respiration correction methods should be investigated, including prospective techniques, but it is important to note that the proposed respiration correction does not degrade data quality or introduce any unexpected effects, as shown in the egg white phantom experiment.

CEST Identifies Signal Changes in MS

The APT effect is driven by proton exchange with exchange rates of 10–300 Hz at an offset frequency of 3.5 ppm from water (5). With a pulse amplitude of 2 μT and duration of 150 ms, the applied saturation field was chosen to be on the order of amide exchange rate, while still being clinically feasible to implement (28,32). Alterations in the CEST z-spectrum in this Δω range were observed in all patients with an EDSS greater than 0, with the most noted changes occurring specifically near the 3.5ppm resonance, rather than throughout the z-spectrum (change in the full width half max or baseline). This indicates that the observed changes in the z-spectrum may be dominated by exchange effects rather than T_1 and T_2 (33). While it has been demonstrated that T_1 signal abnormalities are not as readily apparent in the spinal cord (compared to the brain) of MS patients (34), methods have been proposed to correct for T_1 and the impact of these corrections in MS should be evaluated in future studies (35,36). Nonetheless, these preliminary results indicate that APT CEST may provide information regarding the biochemical composition, and disease evolution in the spinal cord. A previous study has investigated the ability of CEST to observe amine signals (GluCEST) at 7T in the human spinal cord (37). At 3T, the more rapid exchange rates, broader effect and lower concentration of amines make specifically detecting amine contributions to the CEST effect difficult. Nonetheless, the amine-mediated exchange does occur near the APT resonance, and it is important to note that some of the amine effect is captured within the z-spectrum (as seen in Figure 2, where z-spectrum signal differences can be seen in the 2–3 ppm range). While the purpose of this study was to investigate APT effects near 3.5 ppm, future analysis of the entire z-spectrum in healthy controls and patients should be conducted.

The influence of NOE and MT effects is especially important to consider in the MS patient population, where the MT effect is known to be different than in healthy controls (25,26).

These effects, along with relaxation changes (T_1 and T_2) and B_1, influence the APT_w measurement, and thus, in an effort to minimize the contributions of other processes, we looked at the ΔAPT maps. With the ΔAPT maps, only the APT side downfield from water was considered and therefore, any confounding effects from NOE and MT asymmetry were minimized, but the effects from relaxation, other MT and B_1 are still present. We highlight the ΔAPT maps as they provide information of tissue changes relative to healthy volunteers and improve sensitivity for these tissue changes, but at the cost of diminishing specificity. Furthermore, the purpose of the ΔAPT is not to provide an absolute quantification, but instead, to provide a visual inspection of the spatial differences between controls and MS patients, allowing us to identify areas of greatest differences (i.e. primarily in voxels contaminated with partial volume effects at the boundaries of different tissue, localized to lesions, etc.). In doing so, it is apparent that NAWM shows a more dramatic ΔAPT effect than lesions. We hypothesize that at an early stage in the MS pathology (i.e. before a lesion is seen on conventional MRI), the increase in APT effect (larger positive ΔAPT) in NAWM may represent protein accumulation prior to the development of large, inflamed lesions, potentially an early biomarker for tissue damage; furthermore, an increase in APT signal in the NAWM could be caused by increased protein degradation during axonal damage, resulting in higher concentrations of mobile protein and peptide species that contribute to the APT signal. In a more chronic case, such as MS 10 (EDSS = 6), who required walking assistance, a large decrease in ΔAPT is seen throughout the whole cord, corresponding to a more Lorentzian, water-like z-spectrum (38,39). This may be attributed to axonal transection secondary to demyelination, and grossly, a total decrease in tissue microstructure. In MS 3, the increased ΔAPT around the border of the lesions may be indicative of chronic active lesions similar to the ones identified in MS brains (40), where the activated microglia surrounding the lesion margins would show an increase in protein concentration driving the increased ΔAPT (41). It is unclear why a difference in NAWM of MS patients with an EDSS of 0 cannot be as easily detected, but we hypothesize that the disease course in these patients is different and perhaps too premature to allow distinguishing different tissue types. The role of APT in the disease course must be further elucidated, however this study identifies the potential mechanisms APT CEST may be able to unveil in various patients with MS.

Study Limitations

This study was designed so that the maximum SNR was achieved, and therefore, the protocol was not optimized in terms of scan time or total rostral-caudal coverage. In the future, however, scan time reduction via logical restriction of the number of acquired offsets may be feasible. For example, only three averages are needed for the saturated signal to reach steady state and may provide the appropriate SNR for APT quantification, wherein, we utilized five averages. Finally, it is important to emphasize that the APT quantification used in this study was a modified form of the APT asymmetry, considering the area of the z-spectrum (subtracted from 1) on both the positive and negative sides of the spectrum, rather than using a single point. Therefore, the reported signal sizes do not serve as an absolute measurement, and additional quantification methods such as the Lorentzian fitting (16) or a sum of Lorentzian fittings (42), three offset measurement (43), or an inverse z-spectrum analysis to account for T_1 (36) may more accurately reflect and isolate APT changes, warranting future investigation.

Our study provides initial results in exploring the ability of this sequence to detect biologically meaningful changes. It should be noted, however, that a main limitation in this study was not only in the number of patients, but also the severity of disease in these patients. Future longitudinal studies are necessary to determine whether detected changes in the NAWM do indeed precede lesion formation, as hypothesized.

Conclusions

The first application of APT CEST in the cervical spinal cord at 3T has been reported. When adequately correcting for respiratory effects, APT CEST provides information reflective of biochemical changes occurring in the white matter of MS.

Acknowledgments

This study was funded, in part, by the National Multiple Sclerosis Society NMSS RG-1501-02840 (SAS). Additional funding sources include NIH/NINDS R21 NS087465-01 (SAS), NIH/NEI R01 EY023240 (SAS), DoD W81XWH-13-0073 (SAS), and NIH/NIBIB K99/R00 EB016689 (RLB). The authors would like to thank Dr. Kristin O'Grady for her help with scans. We would also like to thank Ms. Kristen George-Durrett, Ms. Clair Jones, Ms. Leslie McIntosh, and Mr. Chris Thompson, who have provided invaluable assistance with scheduling and subject assistance.

References

1. Bot JC, Barkhof F, Polman CH, Lycklama a Nijeholt GJ, de Groot V, Bergers E, Ader HJ, Castelijns JA. Spinal cord abnormalities in recently diagnosed MS patients: added value of spinal MRI examination. Neurology. 2004; 62(2):226–233. [PubMed: 14745058]
2. Kearney H, Miller DH, Ciccarelli O. Spinal cord MRI in multiple sclerosis-diagnostic, prognostic and clinical value. Nat Rev Neurol. 2015; 11(6):327–338. [PubMed: 26009002]
3. Bergers E, Bot JC, De Groot CJ, Polman CH, Lycklama a Nijeholt GJ, Castelijns JA, van der Valk P, Barkhof F. Axonal damage in the spinal cord of MS patients occurs largely independent of T2 MRI lesions. Neurology. 2002; 59(11):1766–1771. [PubMed: 12473766]
4. Bakshi R, Thompson AJ, Rocca MA, Pelletier D, Dousset V, Barkhof F, Inglese M, Guttmann CRG, Horsfield MA, Filippi M. MRI in multiple sclerosis: current status and future prospects. Lancet Neurol. 2008; 7(7):615–625. [PubMed: 18565455]
5. Zhou J, Payen J-F, Wilson DA, Traystman RJ, van Zijl PCM. Using the amide proton signals of intracellular proteins and peptides to detect pH effects in MRI. Nat Med. 2003; 9(8):1085–1090. [PubMed: 12872167]
6. van Zijl PC, Yadav NN. Chemical exchange saturation transfer (CEST): what is in a name and what isn't? Magn Reson Med. 2011; 65(4):927–948. [PubMed: 21337419]
7. Bryant RG. The Dynamics of Water-Protein Interactions. Annu Rev Biophys Biomol Struct. 1996; 25(1):29–53. [PubMed: 8800463]
8. Hua J, Jones CK, Blakeley J, Smith SA, van Zijl PC, Zhou J. Quantitative description of the asymmetry in magnetization transfer effects around the water resonance in the human brain. Magn Reson Med. 2007; 58(4):786–793. [PubMed: 17899597]
9. Sun PZ, Murata Y, Lu J, Wang X, Lo EH, Sorensen AG. Relaxation-compensated fast multislice amide proton transfer (APT) imaging of acute ischemic stroke. Magn Reson Med. 2008; 59(5): 1175–1182. [PubMed: 18429031]
10. Zhou J, Tryggestad E, Wen Z, Lal B, Zhou T, Grossman R, Wang S, Yan K, Fu D-X, Ford E, Tyler B, Blakeley J, Laterra J, van Zijl PCM. Differentiation between glioma and radiation necrosis using molecular magnetic resonance imaging of endogenous proteins and peptides. Nat Med. 2011; 17(1):130–134. [PubMed: 21170048]

11. Jones CK, Schlosser MJ, van Zijl PC, Pomper MG, Golay X, Zhou J. Amide proton transfer imaging of human brain tumors at 3T. Magn Reson Med. 2006; 56(3):585–592. [PubMed: 16892186]
12. Verma T, Cohen-Adad J. Effect of respiration on the B0 field in the human spinal cord at 3T. Magn Reson Med. 2014; 72(6):1629–1636. [PubMed: 24390654]
13. Kurtzke JF. Rating neurologic impairment in multiple sclerosis: an expanded disability status scale (EDSS). Neurology. 1983; 33(11):1444–1452. [PubMed: 6685237]
14. Polman CH, Reingold SC, Banwell B, Clanet M, Cohen JA, Filippi M, Fujihara K, Havrdova E, Hutchinson M, Kappos L. Diagnostic criteria for multiple sclerosis: 2010 revisions to the McDonald criteria. Ann Neurol. 2011; 69(2):292–302. [PubMed: 21387374]
15. Held P, Dorenbeck U, Seitz J, Fründ R, Albrich H. MRI of the abnormal cervical spinal cord using 2D spoiled gradient echo multiecho sequence (MEDIC) with magnetization transfer saturation pulse. A T2* weighted feasibility study. J Neuroradiol. 2003; 30(2):83–90. [PubMed: 12717293]
16. Jones CK, Polders D, Hua J, Zhu H, Hoogduin HJ, Zhou J, Luijten P, van Zijl PCM. In vivo three-dimensional whole-brain pulsed steady-state chemical exchange saturation transfer at 7 T. Magn Reson Med. 2012; 67(6):1579–1589. [PubMed: 22083645]
17. Kim M, Gillen J, Landman BA, Zhou J, van Zijl PCM. Water saturation shift referencing (WASSR) for chemical exchange saturation transfer (CEST) experiments. Magn Reson Med. 2009; 61(6): 1441–1450. [PubMed: 19358232]
18. Heo H-Y, Zhang Y, Lee D-H, Hong X, Zhou J. Quantitative assessment of amide proton transfer (APT) and nuclear overhauser enhancement (NOE) imaging with extrapolated semi-solid magnetization transfer reference (EMR) signals: Application to a rat glioma model at 4.7 tesla. Magn Reson Med. 2016; 75(1):137–149. [PubMed: 25753614]
19. Avants BB, Tustison NJ, Song G, Cook PA, Klein A, Gee JC. A reproducible evaluation of ANTs similarity metric performance in brain image registration. Neuroimage. 2011; 54(3):2033–2044. [PubMed: 20851191]
20. Asman AJ, Bryan FW, Smith SA, Reich DS, Landman BA. Groupwise multi-atlas segmentation of the spinal cord's internal structure. Med Image Anal. 2014; 18(3):460–471. [PubMed: 24556080]
21. Jones CK, Huang A, Xu J, Edden RAE, Schär M, Hua J, Oskolkov N, Zacà D, Zhou J, McMahon MT, Pillai JJ, van Zijl PCM. Nuclear Overhauser enhancement (NOE) imaging in the human brain at 7T. Neuroimage. 2013; 77(0):114–124. [PubMed: 23567889]
22. Birn RM, Diamond JB, Smith MA, Bandettini PA. Separating respiratory-variation-related fluctuations from neuronal-activity-related fluctuations in fMRI. Neuroimage. 2006; 31(4):1536–1548. [PubMed: 16632379]
23. Zhou J, van Zijl PC. Chemical exchange saturation transfer imaging and spectroscopy. Prog Nucl Magn Reson Spectrosc. 2006; 48(2):109–136.
24. Lu J, Zhou J, Cai C, Cai S, Chen Z. Observation of true and pseudo NOE signals using CEST-MRI and CEST-MRS sequences with and without lipid suppression. Magn Reson Med. 2015; 73(4): 1615–1622. [PubMed: 24803172]
25. Smith AK, Dortch RD, Dethrage LM, Smith SA. Rapid, high-resolution quantitative magnetization transfer MRI of the human spinal cord. Neuroimage. 2014; 95(0):106–116. [PubMed: 24632465]
26. Zackowski KM, Smith SA, Reich DS, Gordon-Lipkin E, Chodkowski BA, Sambandan DR, Shteyman M, Bastian AJ, van Zijl PC, Calabresi PA. Sensorimotor dysfunction in multiple sclerosis and column-specific magnetization transfer-imaging abnormalities in the spinal cord. Brain. 2009; 132(Pt 5):1200–1209. [PubMed: 19297508]
27. Dula AN, Asche EM, Landman BA, Welch EB, Pawate S, Sriram S, Gore JC, Smith SA. Development of chemical exchange saturation transfer at 7T. Magn Reson Med. 2011; 66(3):831–838. [PubMed: 21432902]
28. Dula AN, Pawate S, Dethrage LM, Conrad BN, Dewey BE, Barry RL, Smith SA. Chemical exchange saturation transfer of the cervical spinal cord at 7 T. NMR Biomed. 2016
29. Glover GH, Li TQ, Ress D. Image-based method for retrospective correction of physiological motion effects in fMRI: RETROICOR. Magn Reson Med. 2000; 44(1):162–167. [PubMed: 10893535]

30. Birn RM, Smith MA, Jones TB, Bandettini PA. The respiration response function: the temporal dynamics of fMRI signal fluctuations related to changes in respiration. Neuroimage. 2008; 40(2): 644–654. [PubMed: 18234517]

31. Le TH, Hu X. Retrospective estimation and correction of physiological artifacts in fMRI by direct extraction of physiological activity from MR data. Magn Reson Med. 1996; 35(3):290–298. [PubMed: 8699939]

32. Yuan J, Chen S, King AD, Zhou J, Bhatia KS, Zhang Q, Yeung DKW, Wei J, Mok GSP, Wang Y-X. Amide proton transfer-weighted imaging of the head and neck at 3 T: a feasibility study on healthy human subjects and patients with head and neck cancer. NMR Biomed. 2014; 27(10): 1239–47. [PubMed: 25137521]

33. Lee DH, Heo HY, Zhang K, Zhang Y, Jiang S, Zhao X, Zhou J. Quantitative assessment of the effects of water proton concentration and water T1 changes on amide proton transfer (APT) and nuclear overhauser enhancement (NOE) MRI: The origin of the APT imaging signal in brain tumor. Magn Reson Med. 2016

34. Gass A, Filippi M, Rodegher M, Schwartz A, Comi G, Hennerici M. Characteristics of chronic MS lesions in the cerebrum, brainstem, spinal cord, and optic nerve on T1 - weighted MRI. Neurology. 1998; 50(2):548–550. [PubMed: 9484397]

35. Zaiss M, Bachert P. Exchange-dependent relaxation in the rotating frame for slow and intermediate exchange -- modeling off-resonant spin-lock and chemical exchange saturation transfer. NMR Biomed. 2013; 26(5):507–518. [PubMed: 23281186]

36. Zaiss M, Xu J, Goerke S, Khan IS, Singer RJ, Gore JC, Gochberg DF, Bachert P. Inverse Z-spectrum analysis for spillover-, MT-, and T1-corrected steady-state pulsed CEST-MRI – application to pH-weighted MRI of acute stroke. NMR Biomed. 2014; 27(3):240–252. [PubMed: 24395553]

37. Kogan F, Singh A, Debrosse C, Haris M, Cai K, Nanga RP, Elliott M, Hariharan H, Reddy R. Imaging of glutamate in the spinal cord using GluCEST. Neuroimage. 2013; 77(0):262–267. [PubMed: 23583425]

38. Smith S, Bulte PCM, van Z. Direct saturation MRI: Theory and application to imaging brain iron. Magn Reson Med. 2009; 62(2):384–393. [PubMed: 19526497]

39. Mulkern RV, Williams ML. The general solution to the Bloch equation with constant rf and relaxation terms: Application to saturation and slice selection. Med Phys. 1993; 20(1):5–13. [PubMed: 8455512]

40. Bagnato F, Hametner S, Yao B, van Gelderen P, Merkle H, Cantor FK, Lassmann H, Duyn JH. Tracking iron in multiple sclerosis: a combined imaging and histopathological study at 7 Tesla. Brain. 2011; 134(12):3599–3612.

41. Absinta M, Sati P, Reich DS. Advanced MRI and staging of multiple sclerosis lesions. Nat Rev Neurol. 2016

42. Desmond KL, Moosvi F, Stanisz GJ. Mapping of amide, amine, and aliphatic peaks in the CEST spectra of murine xenografts at 7 T. Magn Reson Med. 2014; 71(5):1841–1853. [PubMed: 23801344]

43. Jin T, Wang P, Zong X, Kim SG. MR imaging of the amide - proton transfer effect and the pH - insensitive nuclear overhauser effect at 9.4 T. Magn Reson Med. 2013; 69(3):760–770. [PubMed: 22577042]

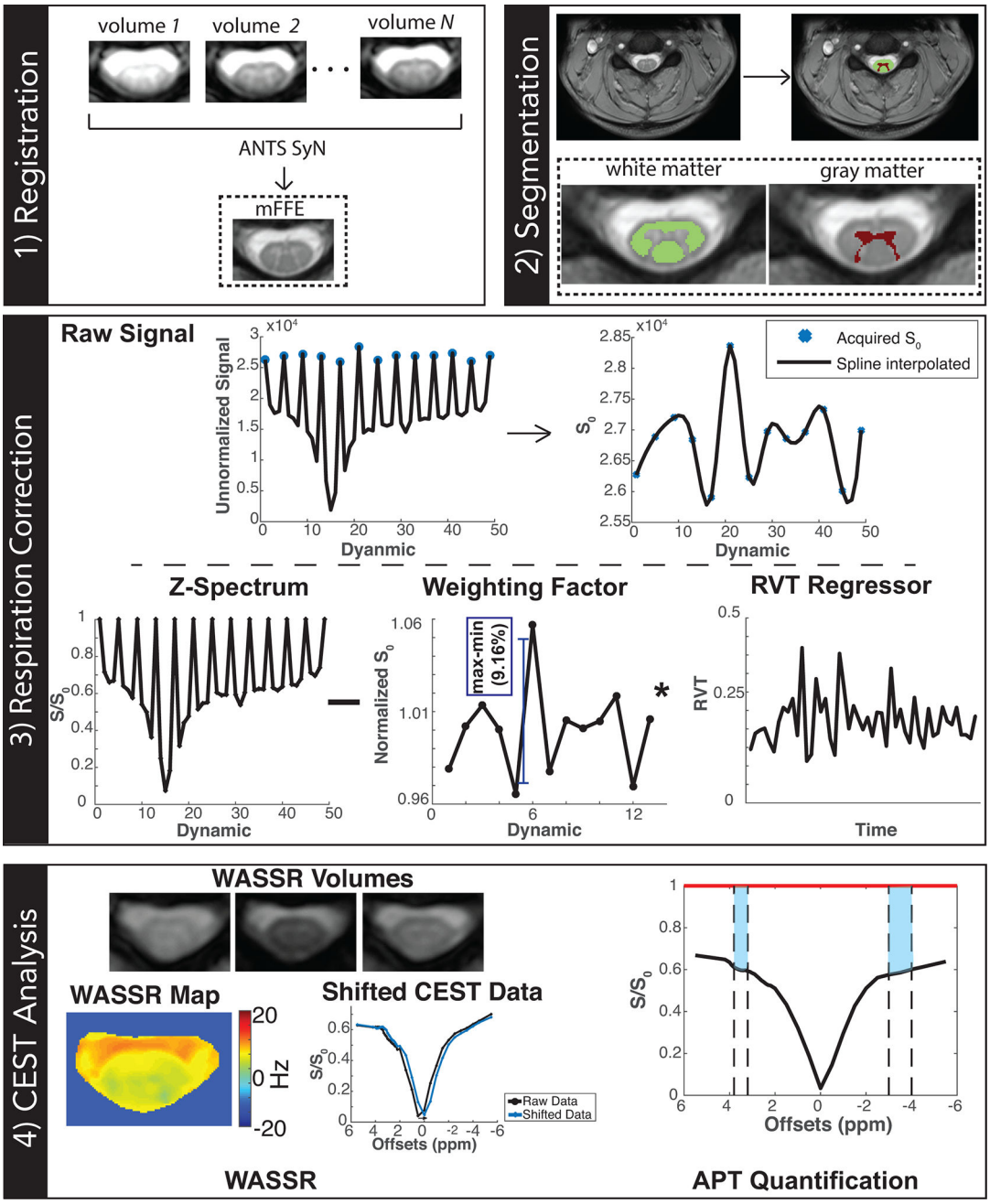

Figure 1. Image Processing Pipeline

The CEST data is registered to the anatomical, which is segmented into white and gray matter. The respiration volume per unit time (RVT) is regressed out of the CEST data, scaled by a weighting factor calculated from the 13 interspersed S_0 images. The resulting z-spectrum is shifted using WASSR.

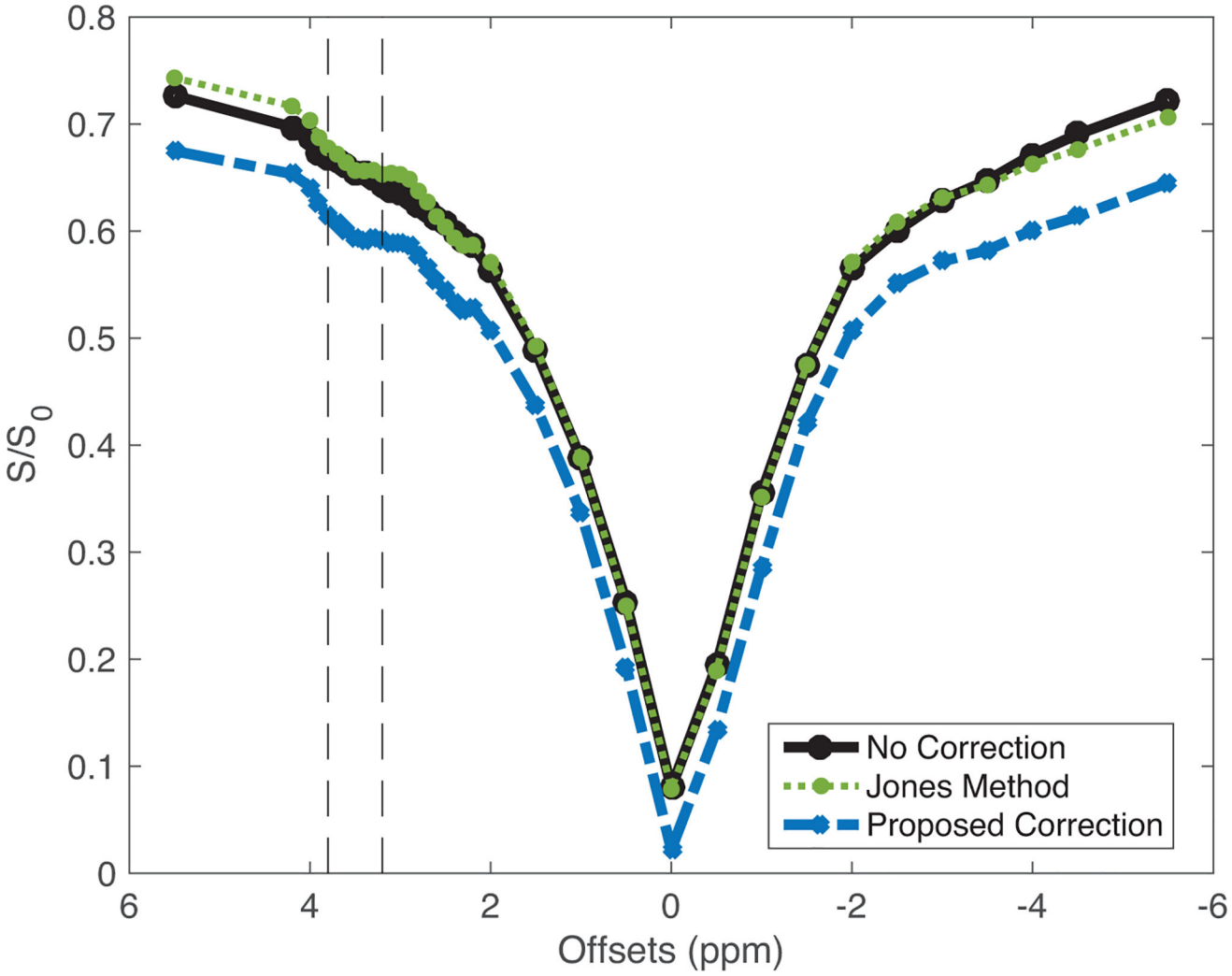

Figure 2. Effect of Respiration Correction in White Matter

Mean z-spectra over all controls without correction (black), with the Jones method correction (green), and with our proposed correction (blue) demonstrate that features in the z-spectrum are confounded by physiological noise. The APT effect can be appreciated when the respiration correction is applied.

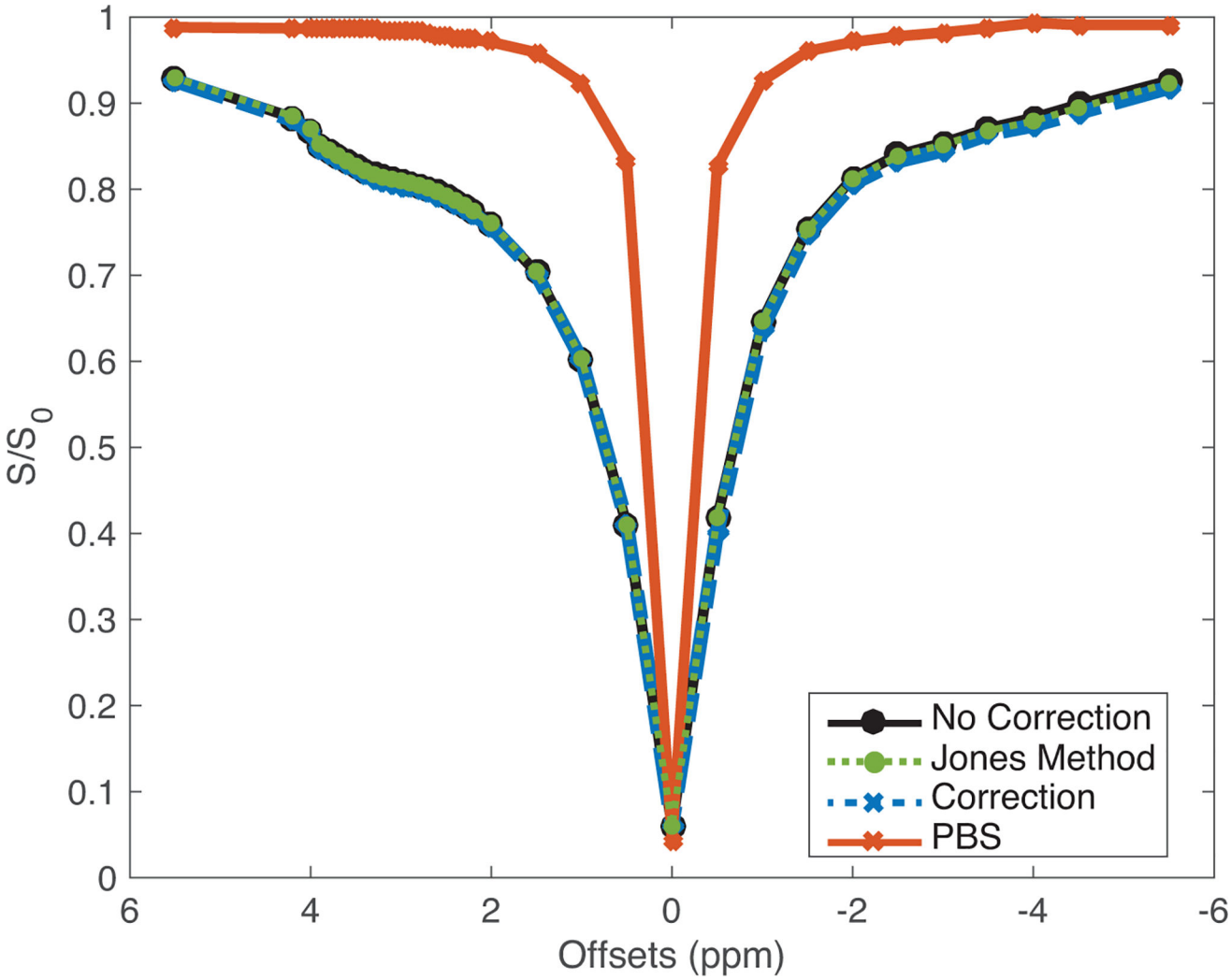

Figure 3. Respiration Correction in Phantom

No adverse effects were produced in the z-spectrum of a non-breathing egg white phantom, as indicated by the good agreement between the z-spectrum of the three comparing methods.

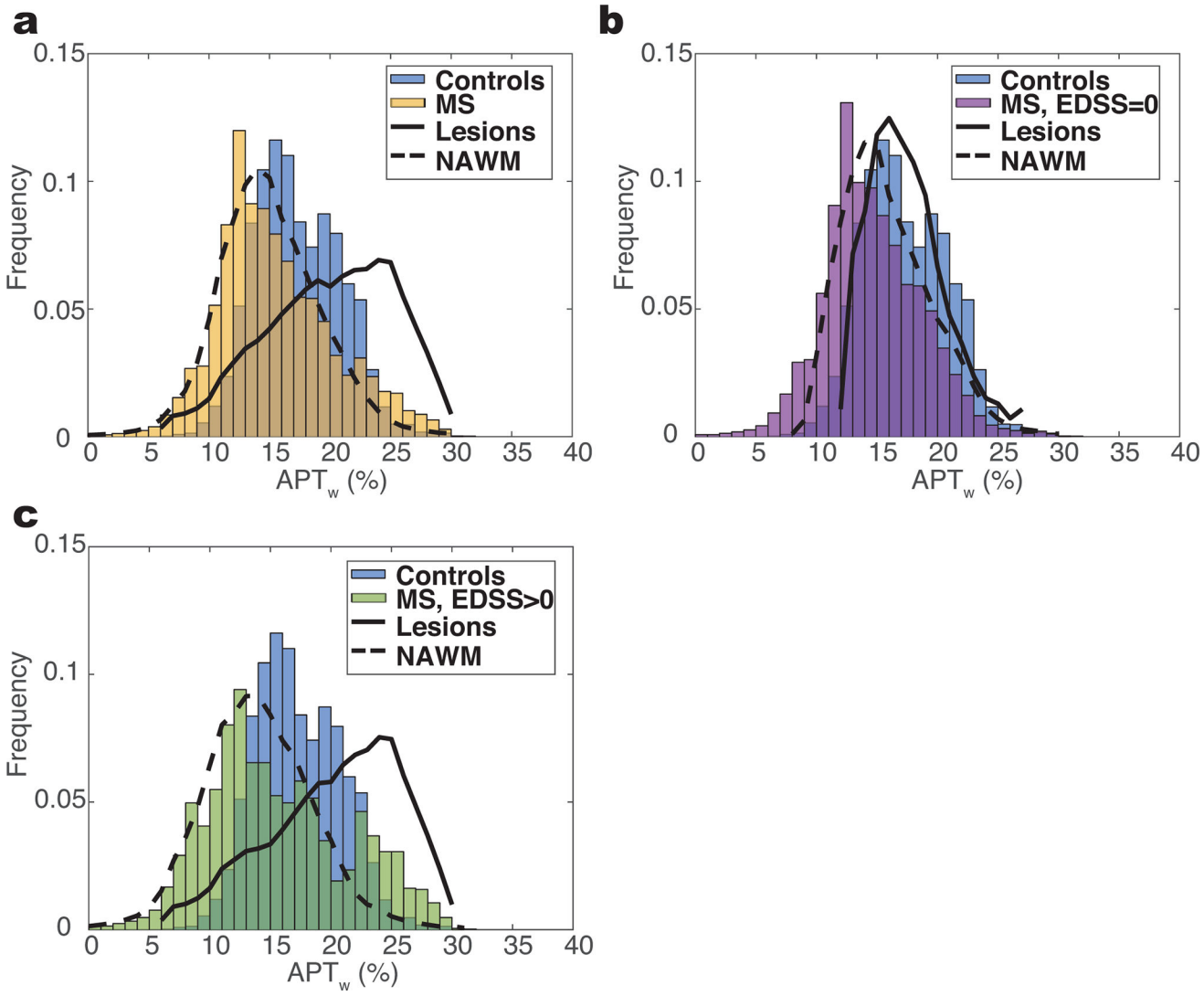

Figure 4. Histogram Analysis of APT_W Measurement

a) Histogram of white matter voxels over all MS patients (yellow) overlaid onto histogram of all controls (blue). b) Large overlap is observed between the controls and MS patients with EDSS of 0 (n=5). c) Patients with an EDSS greater than 0 (green) show a larger deviation from the control histogram and follow a more bimodal distribution, which can be explained by the distributions of distinct types of white matter (lesions vs. NAWM).

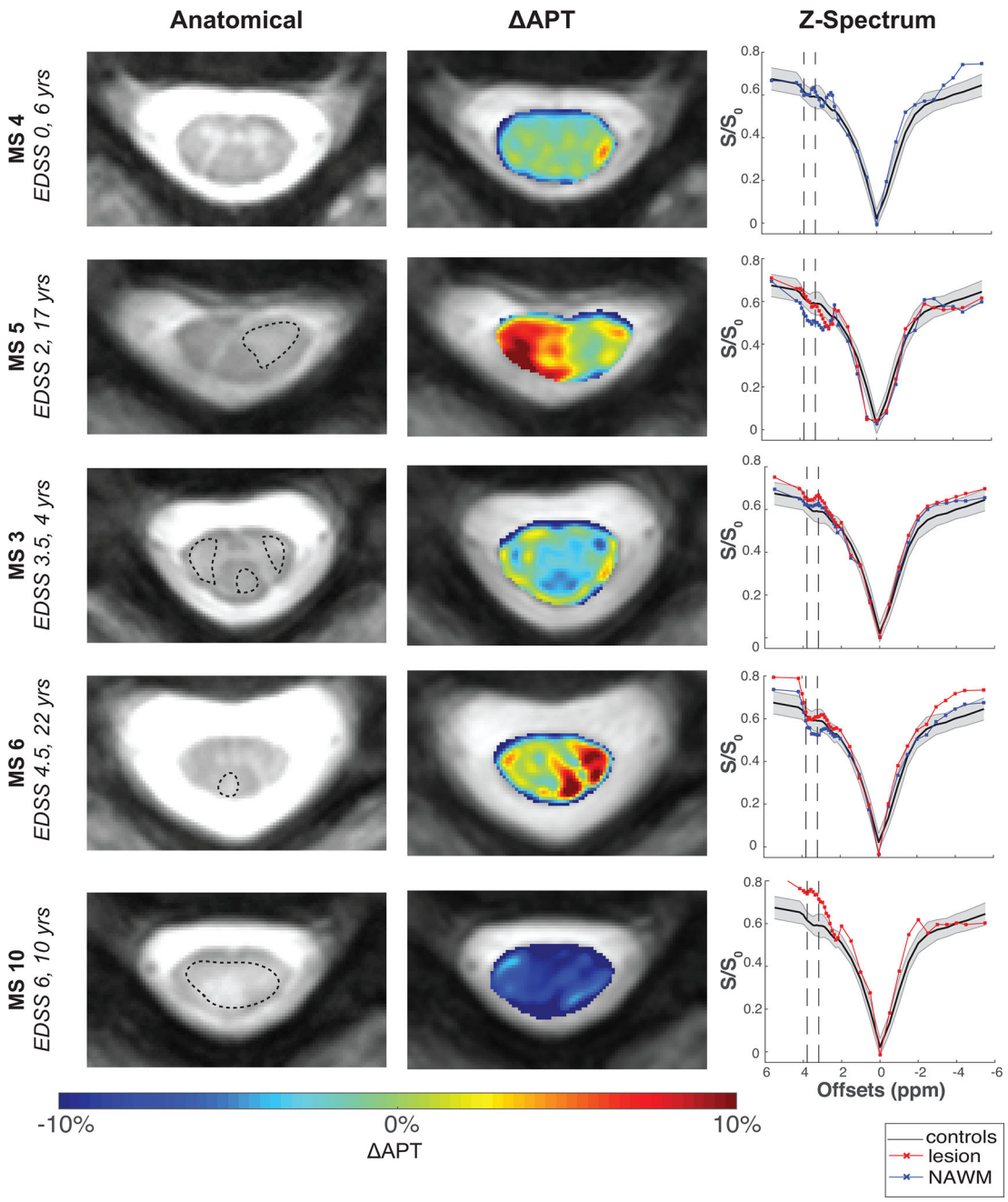

Figure 5. Spatial Characterization of APT in MS Patients

Spinal cord changes in MS patients with varying disease intensity, with anatomical imaging in left column, APT difference maps (ΔAPT) with respect to mean controls in middle column, and corresponding z-spectrum on the right. ΔAPT changes in the NAWM are observed throughout all patients, along with significant heterogeneity between patients.

Table 1

Clinical and Demographic Characteristics of Patients

Patient	Age (years)	Sex	MS Type	MS Duration (years)	EDSS
MS 1	38	F	RRMS	11	0
MS 2	43	F	RRMS	3	0
MS 3	41	F	RRMS	4	3.5
MS 4	40	M	RRMS	6	0
MS 5	46	F	RRMS	17	2
MS 6	58	F	RRMS	22	4.5
MS 7	49	M	RRMS	12	0
MS 8	30	M	RRMS	7	0
MS 9	60	M	PPMS	10	5
MS 10	34	F	RRMS	10	6

Table 2

Overview of APT_w Differences in MS Patients

	All Patients (n=10)		EDSS = 0 (n=5)		EDSS > 0 (n=5)	
Controls WM (n=10)	**NAWM**	**Lesion**	**NAWM**	**Lesion (n=1)**	**NAWM**	**Lesion**
17.5±2.52%	14.4±2.57% P=0.04	16.7±5.66% P=0.96	15.2±2.63% P=0.21	16.8%	13.4±2.5% P=0.04	16.7±6.33% P=0.95